

MODERATELY TO POORLY WELDED TUFF, BISHOP, CALIFORNIA: GEOPHYSICAL AND GEOLOGICAL CHARACTERIZATION TO DETERMINE THE SOURCE OF RADAR SCATTERING.

C. L. Dinwiddie,¹ R. E. Grimm,² R. N. McGinnis,¹ and D. E. Stillman,² ¹Dept. of Earth, Material, and Planetary Sciences, Southwest Research Institute,® 6220 Culebra Road, San Antonio, TX 78238, cdinwiddie@swri.org, ²Dept. of Space Studies, Southwest Research Institute,® 1050 Walnut Street, Suite 300, Boulder, CO 80302.

Introduction: The National Research Council Decadal Study on Terrestrial Analogs to Mars recommended the Bishop Tuff, exposed in the Volcanic Tableland, Bishop, California (Fig. 1), as an analog [1] because some Martian volcanoes and the Stealth region of southwestern Tharsis are thought to be composed of pyroclastic deposits [2–4]. Recent data from the Spirit rover also suggest that the Columbia Hills in part may be of pyroclastic origin [5,6].

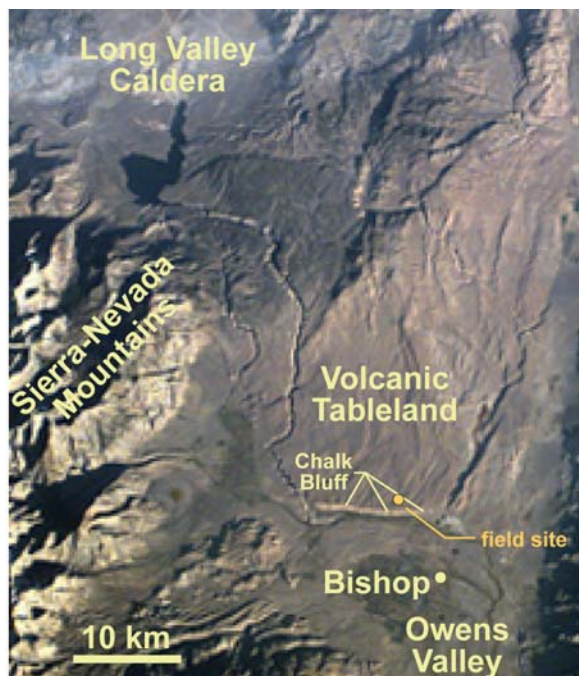


Figure 1. Context image; astronaut photo STS-073, October 25, 1995, Frame 5117, courtesy of Earth Sciences and Image Analysis Laboratory, NASA JSC.

Bishop Tuff: The pumice fall and variably welded rhyolitic ash-flow sheets of the Bishop Tuff are located on the eastern, arid side of the Sierra Nevada mountain range at the north end of Owens Valley (Fig. 1). This tuff was deposited circa 0.76 Ma [7] as a series of pyroclastic flows and falls erupted from the Long Valley Caldera [8], located ~40 km to the northwest of the study area. Quaternary extension is preserved on the surface of the Volcanic Tableland from a series of east- and west-dipping, north-trending normal faults [9]. The southern margin of the Volcanic Tableland is defined by an erosional escarpment (Chalk Bluff) cut by the Owens River, exposing bedded tephra-fall de-

posits, massive tuff units, and several faults in cross-section [10].

Geophysical Investigations: Motivated by interpretations of potential pyroclastic deposits on Mars [2–4] and the possibility that low-frequency MARSIS and SHARAD orbital sounding radars could soon be probing such deposits, we began geophysical surveys of the Bishop Tuff in June 2004.

Transient Electromagnetic Surveys. Given that ground-penetrating radar (GPR) has limited utility in low resistivity environments, we decided to conduct *in situ* resistivity soundings and perform laboratory analyses of field samples in advance of GPR surveys to first determine if the Bishop Tuff was geoelectrically amenable to use of GPR. We determined the resistivity of the bulk unsaturated tuff sequence to be relatively high (on order of 1000 Ω -m) using transient electromagnetic methods (TEM) with 50- to 100-m loops, but also identified the need to investigate the resistivity of the very near surface (i.e., shallower than ~30 m) using methods like Schlumberger direct-current (DC) vertical electrical soundings to provide critical near-surface data for estimating GPR signal attenuation due to absorption.

Vertical Electrical Soundings and Low-frequency GPR Surveys. The resistivity results from initial TEM soundings were encouraging enough for us to return to Bishop in November 2004 with DC resistivity, low-frequency GPR (12.5–80 MHz), and TEM equipment. Joint inversion [11] of vertical electrical sounding and TEM sounding data revealed that the near surface (2–30 m deep) was characterized by more highly conductive units (400–800 Ω -m, depending upon location) than previously estimated for the bulk subsurface using TEM data alone. Our low-frequency radar profiles suggested that the moderately welded caprock zone and the underlying sintered zone and non- to poorly welded zone of unit IG2Eb [12] are a source of abundant discrete scatterers. Vertical density variations in the Bishop Tuff are due to its depositional thermal and welding history. These low-frequency radar soundings yielded absorption attenuation of ~1 dB/m and strong scattering attenuation of ~1 dB/m [13]. In the absence of detailed geological characterization studies at that time, we noted similarity between our pulseEKKO (pE) radar profiles and a 50-MHz pE profile from the Tumalo Tuff, Oregon [14]; we reached the preliminary

conclusion that discrete scatterers observed in our data were perhaps a result of welding density heterogeneities [12]. We also suggested that contrasts in dielectric constant due to contrasts in density could be further enhanced by contrasts in moisture content [12].

Geological Characterization, Multielectrode Resistivity Profiling, and Higher-Frequency GPR Surveys. We returned to the Volcanic Tableland in July 2006 with a differential GPS system, multielectrode resistivity, and higher-frequency GPR (50–900 MHz) to better assess the source of near-surface scattering. Returning to the second of our previous [12] test sites (Site 2), we used the 10-channel, 96 electrode Syscal Pro (IRIS) resistivity meter and the Sensors and Software pE 100 GPR with 50, 100, 200 MHz antennas to scan the subsurface. GSSI data were collected with 270, 500, and 900 MHz antennas. We performed differential GPS-based structural geological mapping of the local outcropping tuff surface and collected rock and alluvium/colluvium samples for laboratory-based specific gravity and EM property analyses.

Site Description: Site 2 is located on an unimproved road at northing 4142361, easting 372273, elev. 1351.1 m amsl, datum UTM NAD 83 zone 11; this road passes by the only domicile on the Volcanic Tableland. Given a stratigraphic column measured nearby at Chalk Bluff [10], we extrapolate that the radar imageable portion of the subsurface below the study site consists of ~10 m of moderately welded to sintered Bishop Tuff grading below this depth to poorly welded tuff. The road surface is characterized by in-place blocks bounded by a polygonal network of cooling joints.

Joint inversion of 1D VES and TEM data indicates the shallow subsurface of this site is characterized by resistivities of ~850 $\Omega\cdot\text{m}$ from a depth of 1 to 31 m below the surface and that the site overlies a relatively thick unsaturated zone (Fig. 2).

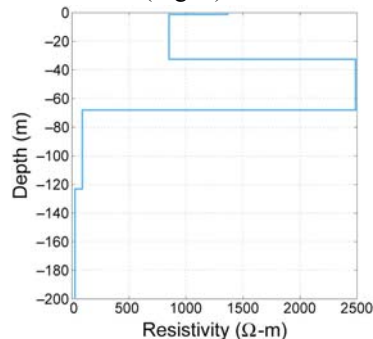


Figure 2. TEM/VES joint inversion model of subsurface resistivity with depth for Site 2.

Samples for analysis of lateral variation in volcanic tuff properties were collected from the northwestern edge of the road on 5-m-centers and also from a few

extra site-specific tuff samples along a total transect length of 100 m ($n_{\text{tuff}} = 24$). Laboratory analysis yielded a moderately welded tuff particle density of 2.10 ± 0.10 g/cc, bulk density of 1.58 ± 0.14 g/cc, and porosity of 0.25 ± 0.07 .

GPR surveys (2004 and 2006) and the multielectrode resistivity survey were conducted with transects along the road, oriented parallel to the road and approximately perpendicular to predominant fault trend. Resistivity data from 48- and 96-electrode arrays were collected along a ~95-m-long transect on the northwestern edge of the road. GPR data (50, 100, and 200 MHz antennas in two polarizations) were obtained from four ~95-m-long parallel transects and a fifth, shorter, parallel transect along the road; all transects were separated laterally by no more than 3.5 m, and three transects were separated by only 10 cm (3 of 5 GPR transects shown in Fig. 3).

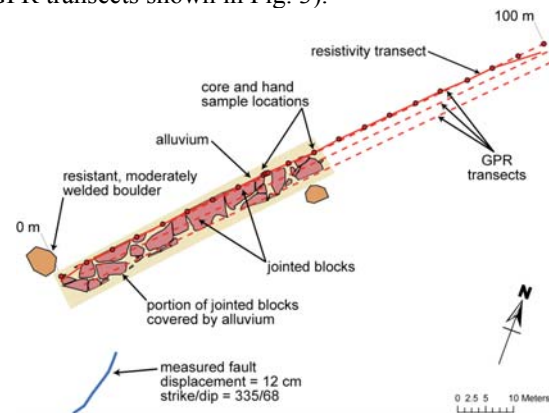


Figure 3. Survey configuration at Site 2, including structural geological map of southwest end of survey site.

Results: For the remainder of this paper we focus on resistivity and 200 MHz GPR data from the transect along the northwestern edge of the road.

Geological Characterization. Cooling joints filled with unconsolidated material were mapped on the road using differential GPS. These joints form a polygonal network that defines in-place blocks in the road bed (Fig. 3). We have no definitive data to confirm the vertical extent of the cooling joints at Site 2, but we expect an overall decrease in cooling joint abundance with depth because of the transition from moderately welded to more poorly welded tuff. Nearby vertical exposures along Chalk Bluff and within an incised paleochannel suggest that cooling joints of this style are best developed in the upper ~10 m of capping moderately welded tuff [15]. We also mapped a fault in the moderately welded caprock ~10 m south of the road (Fig. 3).

Multielectrode Resistivity Profiles. As indicated by 2D resistivity profiles (Fig. 4), resistivity structure at this site is laterally heterogeneous and complex. Hot

colors (reds) are interpreted to represent the interior of intact tuff blocks. Near-surface cool (blues) to mid-range colors (greens) are interpreted to represent unconsolidated fracture filling material within open fractures between blocks of tuff. Mid-range colors may also be interpreted as relatively weathered tuff. In comparison, although a 1D joint inversion model of our TEM and VES data from 2004 (Fig. 2) captured the average resistivity of the near surface, it was not sufficient to capture the complex resistivity structure revealed in multielectrode resistivity profiles, nor did it adequately explain the lateral complexity revealed in low-frequency radar profiles from 2004.

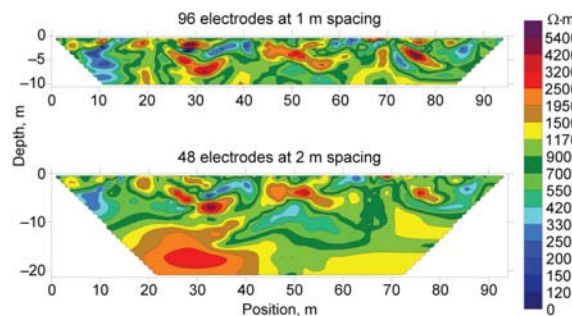


Figure 4. Resistivity profiles as modeled from data collected with 96-electrode and 48-electrode arrays.

Radargrams. Inverted V-shapes (i.e., Λ) characterize the near-surface returns in unmigrated pE radargrams; in many cases, the apex coincides with mapped geologic contacts between tuff blocks and alluvium or colluvium fill material (Fig. 5). Sometimes both legs of the Λ are not fully apparent, which may be due to suboptimal antenna ground coupling in certain locations. The Λ s do not always have identical slopes, which is likely because the transect is not always perpendicular to local joints and because joint dip angles vary from one location to another. We interpret the signature Λ to represent a reflected, subhorizontal, near-surface wave interacting with near-surface and subvertical geologic contacts.

In contrast, we interpret semicontinuous to discrete subhorizontal signatures to indicate localized primary cooling joints, secondary unloading joints, or perhaps topographic expression of units below (Fig. 5). We observe such signatures in both radar and resistivity data.

Correlation of Resistivity with Radar. When we superimpose the unmigrated radar and resistivity data, we note correlation between major, bounding reflectors and localized zones exhibiting high and low resistivity (Fig. 6).

Migrated Data. Migration removes the near-surface scattering signatures for the most part, making interpretation of subhorizontal reflectors somewhat

easier (Fig. 7). Large-scale curving reflectors may indicate irregular morphology of the interface between the moderately welded capping tuff and deeper units.

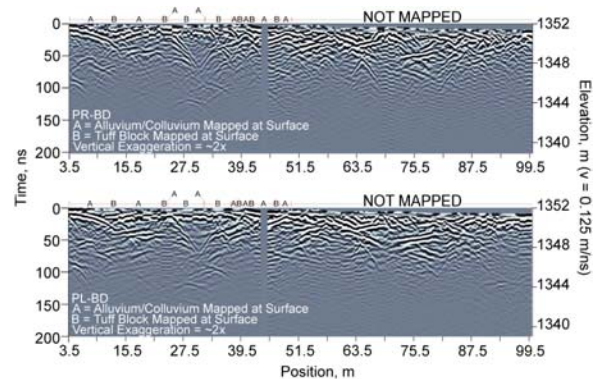


Figure 5. 200 MHz radargrams (unmigrated) of transect on northwestern edge of road. Traces are missing at an obstruction. PR-BD and PL-BD indicate perpendicular and parallel (to transect) broadside antenna polarizations. CMP analysis yields $v = 0.125$ m/ns. Polygonal cooling joints mapped at the surface are indicated as the interface between A (fill material) and B (tuff block) for the first ~ 50 m of the transect.

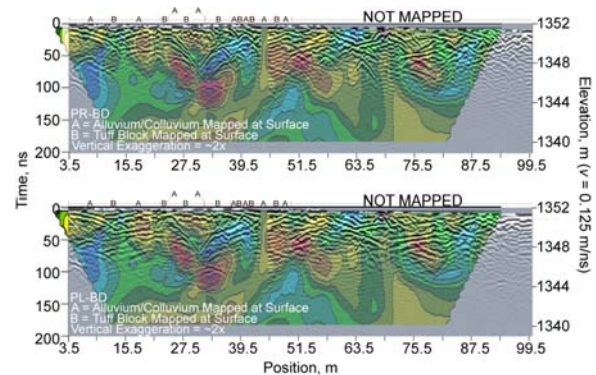


Figure 6. Layered diagram superimposing 200 MHz radargram on resistivity. Polygonal cooling joints mapped at the surface are indicated as the interface between A and B, as in Fig. 5.

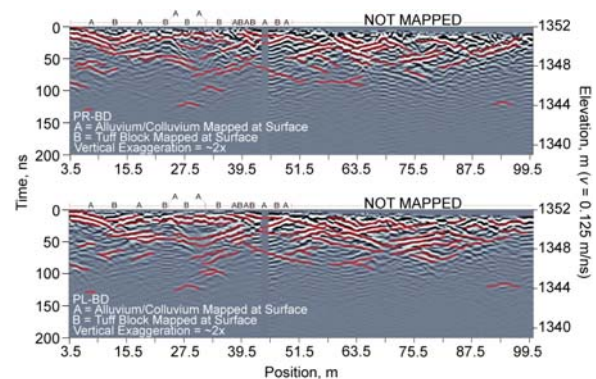


Figure 7. Migrated 200 MHz radargrams. Deepest reflection lies at ~ 8 m. Polygonal cooling joints mapped at the surface are indicated as the interface between A and B, as in Fig. 5.

Conclusions: Our results suggest that structural deformation in the form of a polygonal network of cooling joints in the moderately welded caprock and perhaps in underlying units is the likely source of near-surface scattering in radar profiles. Subvertical cooling joints, exposed at the surface, may be interpreted in the subsurface and should provide fluid pathways to pond percolating water or promote conduit flow. Ponding water will promote erosion and dissolution both vertically and horizontally, further segmenting joint-bounded blocks of tuff. Unexposed faults may also be present, given the regional structure of the area and our observation of a fault at the surface ~10 m south of the road. Diffractions in the form of Λ appear to coincide with mapped geologic contacts between tuff blocks and unconsolidated fracture filling material—supporting an interpretation that this signature represents a reflected, subhorizontal, near-surface wave interacting with near surface geologic contacts. Semi-continuous to discrete, subhorizontal signatures in radargrams may be indicative of localized primary cooling joints or secondary unloading joints. Large-scale curving reflectors may indicate irregular morphology of the transitional base of the capping moderately welded tuff.

As mentioned previously, we had noted the similarity between diffraction hyperbolas in our low-frequency radar profiles and those in a 50-MHz pE profile of the Tumalo Tuff [14] and formed a preliminary hypothesis that the diffractors observed in our own pE profiles were perhaps a result of welding density heterogeneities [13]. Using higher frequency GPR and our own geologic maps, we now conclude that diffractors in radargrams of the Bishop Tuff primarily result from density and mineralogical contrasts between intact tuff blocks and fracture-filling unconsolidated sedimentary material (perhaps also from air pockets between horizontally segmented tuff blocks) and are to a lesser degree affected by welding heterogeneities. We had also suggested that contrasts in dielectric constant due to contrasts in density could be further enhanced by contrasts in moisture content [13]. Because percolating water will move preferentially within joints filled with granular material rather than within fairly impermeable tuff blocks, the moisture content within joints should also be locally significantly higher than within intact tuff, such that dielectric contrasts would indeed be strengthened. Finally, we posit that perhaps the Tumalo Tuff, although in general significantly less welded than the upper surface of the Bishop Tuff, does exhibit broad and irregular joints that may be on par with the scale of joints measured at Site 2 [16], especially at its cliff-forming exposures [16]; radar teams who have worked at the

Tumalo Tuff might consider whether their data is consistent with jointed tuff.

While the resistivity of the Bishop Tuff is moderately high by Earth standards, these deposits do not serve as exceptionally good geophysical analogs to Mars given the extremely high resistivities expected for the desiccated Martian subsurface. Cooling joints are common to basalts as well as pyroclastic deposits, however, so the geological analogy of the Bishop Tuff remains a compelling one. As we continue use of broadband radar to investigate the frequency-dependence of radar signatures [e.g., 13, 17], our geological and geophysical characterization of the three-dimensional nature of pyroclastic deposits perforated throughout with cooling joints should enhance the technical basis for future interpretation of Mars' orbital, and especially rover- and lander-based GPR data from geologic units characterized by cooling joints in pyroclastic or basaltic rocks.

Acknowledgements: This work was supported by SwRI's Southwest Initiative for Mars (SwIM™) internal research program under contracts R9470 and R9499 in 2004, and by NASA Mars Fundamental Research award no. NNG05GM32G from 2005 to 2007. Any opinions, findings, and conclusions or recommendations expressed in this paper are those of the authors and do not necessarily reflect the views of the National Aeronautics and Space Administration.

The authors thank S. Sandberg and D. Farrell for joint inversions of TEM/VES data, A. Morris for his technical review of this paper, and the following persons for field support: E. Heggy, D. Bannon, S. Gonzalez, B. Winfrey, and D. Wyrick. K. Bradbury and E. Heggy, respectively, performed specific gravity and dielectric measurements of rock and alluvium samples.

References: [1] Farr T. et al. (2001) NRC, Washington D.C. [2] Edgett K. S. et al. (1997) *JGR*, 102, 21545–21568. [3] Scott D. H. and Zimbelman J. R. (1995) U.S.G.S. Misc. Geologic Investigation Map I-2480. [4] Zimbelman J. R. (2003) GSA Annual Meeting, Abstract #98-7. [5] McSween H. Y. et al. (2006) *JGR*, 111(E9), doi: 2006JE002698 [6] Squyres S. W. et al. (2006), *JGR*, 111(E2), doi: 2005JE002562. [7] Sarna-Wojcicki A. et al. (2000) *JGR*, 105, 21,431–21,443. [8] Pinter N. (1995) *J. Geol.*, 103, 73–83. [9] Ferrill D. A. et al. (1999) *J. Struct. Geol.*, 21, 1,027–1,038. [10] Evans J. P. and Bradbury K. K. (2004) *Vadose Zone J.*, 3, 602–623. [11] Sandberg S. K. (1990). New Jersey Geol. Surv. Open-File Report OFR90-1. [12] Wilson C. J. N. and Hildreth W. (1997) *J. Geology*, 105, 407–439. [13] Grimm R. E. et al. (2006) *JGR*, 111, 2005JE002619. [14] Rust A. C. and Russell J. K. (2000) *J. Volcanol. Geotherm. Res.*, 95, 23–34. [15] Ferrill D. A. (2007) Southwest Research Institute, personal communication. [16] Hill B. E. (2007) U.S. Nuclear Regulatory Commission, personal communication. [17] Grimm R. E. and Stillman D. E. (2007) 7th International Conference on Mars.